Quantitative Analysis of Dynamic ^{123}I-mIBG SPECT Imaging Data in Healthy Humans with a Population-Based Metabolite Correction Method

Jing Wu[1], Shu-fei Lin[1], Jean-Dominique Gallezot[1], Chung Chan[1], Rameshwar Prasad[1], Stephanie L. Thorn[2], Mitchel R. Stacy[2], Yiyun Huang[1], Taraneh Hashemi Zonouz[2], Yi-Hwa Liu[2–4], Rachel J. Lampert[2], Richard E. Carson[1], Albert J. Sinusas[1,2], and Chi Liu[1]

[1]Department of Radiology and Biomedical Imaging, Yale University, New Haven, Connecticut; [2]Department of Internal Medicine (Cardiology), Yale University, New Haven, Connecticut; [3]Department of Biomedical Imaging and Radiological Sciences, National Yang-Ming University, Taipei, Taiwan; and [4]Department of Biomedical Engineering, Chung Yuan Christian University, Taoyuan, Taiwan

Conventional 2-dimensional planar imaging of ^{123}I-metaiodobenzylguanidine (^{123}I-mIBG) is not fully quantitative. To develop a more accurate quantitative imaging approach, we investigated dynamic SPECT imaging with kinetic modeling in healthy humans to obtain the myocardial volume of distribution (V_T) for ^{123}I-mIBG. **Methods:** Twelve healthy humans underwent 5 serial 15-min SPECT scans at 0, 15, 90, 120, and 180 min after bolus injection of ^{123}I-mIBG on a hybrid cadmium zinc telluride SPECT/CT system. Serial venous blood samples were obtained for radioactivity measurement and radiometabolite analysis. List-mode data of all the scans were binned into frames and reconstructed with attenuation and scatter corrections. Myocardial and blood-pool volumes of interest were drawn on the reconstructed images to derive the myocardial time–activity curve and input function. A population-based blood-to-plasma ratio (BPR) curve was generated. Both the population-based metabolite correction (PBMC) and the individual metabolite correction (IMC) curves were generated for comparison. V_T values were obtained from different compartment models, using different input functions with and without metabolite and BPR corrections. **Results:** The BPR curve reached the peak value of 2.1 at 13 min after injection. Parent fraction was approximately 58% ± 13% at 15 min and stabilized at approximately 40% ± 5% by 180 min after injection. Two radiometabolite species were observed. When the reversible 2-tissue-compartment fit was used, the mean V_T value was 29.0 ± 12.4 mL/cm^3 with BPR correction and PBMC, a 188% ± 32% increase compared with that without corrections. There was significant difference in V_T with BPR correction ($P = 2.3\text{e-}04$) as well as with PBMC ($P = 1.6\text{e-}05$). The mean difference in V_T between PBMC and IMC was −3% ± 8%, which was insignificant ($P = 0.39$). The intersubject coefficients of variation after PBMC (43%) and IMC (42%) were similar. **Conclusion:** The myocardial V_T of ^{123}I-mIBG was established in healthy humans for the first time. Accurate kinetic modeling of ^{123}I-mIBG requires both BPR and metabolite corrections. Population-based BPR correction and metabolite correction curves were developed, allowing more convenient absolute quantification of dynamic ^{123}I-mIBG SPECT images.

Metaiodobenzylguanidine labeled with ^{123}I (^{123}I-mIBG) is a norepinephrine analog that has a reuptake mechanism similar to that of norepinephrine without being catabolized in the myocardial sympathetic nerve endings and has been the most widely used sympathetic innervation imaging agent in research and clinical studies for risk stratification of patients with congestive heart failure (HF) (*1–5*). For conventional ^{123}I-mIBG imaging, early (15–30 min) and delayed (3–5 h) 2-dimensional (2D) planar images are typically acquired and used for calculating heart-to-mediastinum ratio (HMR) and washout rate (WOR). However, 2D planar imaging is not fully quantitative, because of the superposition of background structures with the 2D heart region of interest and lack of corrections for attenuation and scatter. Three-dimensional (3D) SPECT ^{123}I-mIBG imaging has been proposed to overcome this limitation and enable evaluation of regional myocardial tracer uptake (*6–11*). However, the HMR and WOR values change with the timing for early and delayed imaging in both 2D planar and 3D SPECT, which are only surrogates of tracer retention and kinetics. The ultimate solution for accurate quantification of myocardial ^{123}I-mIBG uptake may lie in the use of 4-dimensional (4D) dynamic SPECT imaging through application of tracer kinetic modeling that can provide intrinsic physiologic parameters, which are independent of the imaging time points. Early studies with traditional rotating cameras (*12*) and recent studies with new stationary cadmium zinc telluride (CZT) scanners (*13,14*) have proposed the use of dynamic ^{123}I-mIBG SPECT imaging to obtain additional kinetic information. However, short acquisition times or lack of accurate data corrections in these studies prevented reliable quantification of ^{123}I-mIBG kinetics.

To develop a potentially more sensitive and accurate approach for absolute quantitation of ^{123}I-mIBG imaging, we investigated 4D dynamic SPECT imaging on a stationary dedicated cardiac CZT SPECT/CT scanner and investigated tracer kinetic modeling

in healthy humans to derive the normal value of volume of distribution (V_T) of ^{123}I-mIBG, which is defined as the ratio of tracer activity concentration in the myocardium to that in the plasma at equilibrium and has been used as a gold standard for quantification of receptor density (15). Thus, V_T can be used as the appropriate parameter for quantification of the norepinephrine transporter density, which can provide insight into ^{123}I-mIBG retention and cardiac sympathetic activity. In this study, metabolite analysis of ^{123}I-mIBG was performed, and a population-based metabolite correction method was proposed for 4D dynamic ^{123}I-mIBG imaging.

MATERIALS AND METHODS

Study Subjects and Imaging Protocol

This study included 12 healthy human volunteers (7 men and 5 women) between the ages of 32 and 64 y (48 ± 13 y) with a body mass index between 22.8 and 38.1 kg/m^2 (28.0 ± 5.3 kg/m^2), free of heart disease or other significant illnesses or medications that could influence sympathetic activity of the heart. Pregnancy or cognitive impairment were exclusions. All subjects had a normal resting 12-lead electrocardiogram. The study was approved by the institutional review board, and all subjects signed an informed consent form.

All subjects received an intravenous bolus injection of 233 ± 67 MBq of ^{123}I-mIBG (AdreView; GE Healthcare) over 20 s. Five 15-min dynamic SPECT scans were acquired starting at 0, 15, 90, 120, and 180 min after injection on a stationary dedicated cardiac hybrid CZT SPECT/CT scanner (Discovery NM/CT 570c; GE Healthcare). The subjects remained in the scanner for the first 2 scans and then left the scanner to take breaks between the following scans. CT scan was acquired for attenuation correction.

Image Generation

List-mode SPECT data of all 5 scans were binned into 29 frames (15 × 20 and 14 × 300 s). The CT image was aligned with the reconstructed SPECT image without attenuation correction on the Xeleris workstation (GE Healthcare) using an attenuation correction quality control protocol to create an aligned attenuation map for subsequent reconstruction with attenuation correction for each scan. A scatter-correction method incorporating the low-energy tail effects of the CZT detector into the projection-based spatial-spectral scatter model, which was previously developed in our group for this CZT SPECT scanner, was applied (16). A maximum-likelihood expectation maximization algorithm with 80 iterations was used to reconstruct all dynamic images using an offline program (17). A postreconstruction 3D Butterworth filter was applied to each image (order = 7, cutoff frequency = 0.37 pixel^{-1}).

Blood Analysis

Sequential discrete venous blood samples taken at 3, 8, 15, 30, 60, 90, 120, and 180 min after injection were used for radioactivity concentration measurements, and plasma samples were analyzed for unmetabolized ^{123}I-mIBG fraction with an automatic column-switching high-performance liquid chromatography system as described in a previous publication (18) eluting with a mobile phase of 27% acetonitrile and 73% 0.1 M (v)/(v) at a flow rate of 1.40 mL/min. The unmetabolized parent fraction was determined as the ratio of the radioactivity of the parent to the total amount of radioactivity collected, normalized by the fitted extraction efficiency (exponential fit), which was determined by corresponding reference plasma samples.

Kinetic Modeling

Volumes of interest (VOIs) were manually drawn on 7 consecutive transverse slices for the myocardium and 4 or 5 slices for the blood pool in dynamic SPECT images using the middle 5-min data. For each subject, VOIs of each scan were generated separately with the same VOI volume.

The mean voxel number was 366 ± 88 in myocardial VOIs and 44 ± 8 in blood-pool VOIs for all 12 subjects. Activity concentrations in the blood pool and myocardium were decay-corrected to obtain the image-derived input function and myocardial time–activity curve for kinetic modeling.

A population-based blood-to-plasma ratio (BPR) curve was generated using a 2-exponential plus constant function to fit the ratio data from all 12 subjects. BPR correction was implemented by dividing the image-derived input function by the BPR curve.

Both population-based metabolite correction (PBMC) and individual metabolite correction (IMC) were performed for comparison. IMC was determined by a 2-exponential fit. PBMC was obtained by fitting the parent fraction data of all the other 11 subjects (leave-1-out), also using a 2-exponential function, and applied to each study.

Tracer kinetic modeling was performed using various input functions as described below to fit the myocardial time–activity curve for each subject. Parameters of the compartment models (19) were estimated using weighted least squares with a Marquardt–Levenberg algorithm (20). A blood volume term was included in all models to correct for spill-in from the left ventricle blood pool. The weights were calculated for each frame using Equation 1:

$$\text{Weight} = \frac{L^2}{C \times DCF^2}, \qquad \text{Eq. 1}$$

where L is the frame duration, C is the total count number, and DCF is the decay-correction factor for each frame.

One-tissue (1T)-reversible 2-tissue (2T), and irreversible 2-tissue (2Ti)-compartment models were investigated to identify the optimal model for ^{123}I-mIBG kinetics. The Akaike information criterion values of these compartment models were calculated. To evaluate the effect of both BPR correction and metabolite correction on the kinetic modeling results, V_T values were obtained from the optimized compartment model using different input functions: without any correction, with BPR correction only, with PBMC only, with both BPR correction and PBMC, and with both BPR correction and IMC.

Statistical Methods

To evaluate the difference should be "n−1" between the PBMC and IMC curves, the SD of the IMC curves with respect to the PBMC curve at different time points were calculated as:

$$\sqrt{\frac{1}{n-1} \sum_{i=1}^{n} (IMC_i(t) - PBMC(t))^2}, \qquad \text{Eq. 2}$$

where $n = 12$ is the number of subjects, $IMC_i(t)$ is the IMC curve value for the i-th subject at the time point t, and PBMC(t) is the PBMC curve value at the time point t. The PBMC curve used here was fitted using the parent fraction data of all subjects. Comparisons between V_T values derived using different input functions were conducted using the paired t test.

RESULTS

Tracer Distribution in Dynamic Images

Sample reconstructed dynamic ^{123}I-mIBG transaxial images in 1 subject are shown in Figure 1. The dynamic images show that the radiotracer entered into the right ventricle blood pool shortly (20–40 s) after the injection and then occupied both ventricle blood pools during 40–60 s. The radiotracer cleared from the blood pools and penetrated into the myocardium within 2 min after the injection. At late phases, ^{123}I-mIBG was retained in the myocardium, as expected.

Venous Blood Sample Analyses

As shown in Figure 2, a BPR curve was generated by fitting all the BPRs collected from 12 subjects. The fitted BPR curve
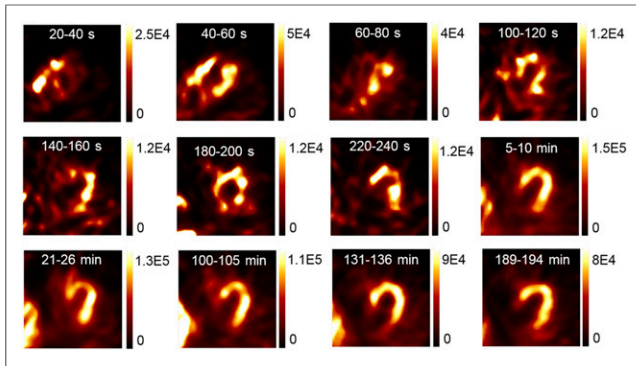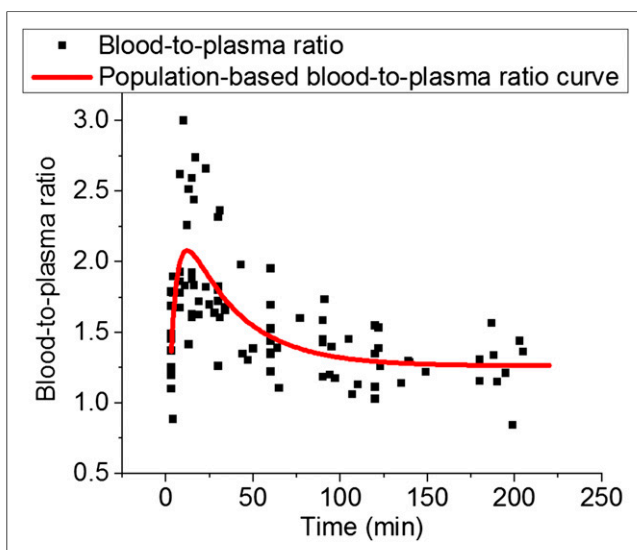
FIGURE 1. Sample transaxial dynamic SPECT images of ^{123}I-mIBG for healthy human. Each image is scaled to its own maximum value (unit: counts, without corrections for decay and frame duration).
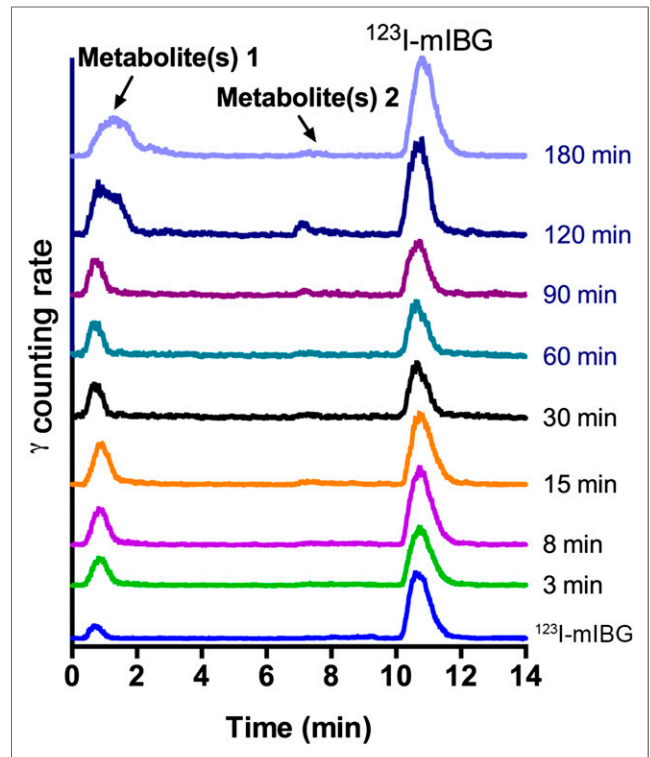
reached the peak value of 2.1 at approximately 13 min after injection. The BPR then declined and stabilized at approximately 1.3 after 120 min after injection.

An example of serial radiochromatograms of venous plasma samples for 1 subject is shown in Figure 3. Two radiometabolite peaks can be observed with earlier retention times (1 major peak with retention time of ~1 min at all time points, and 1 minor peak with retention time of ~7 min at later time points) in comparison with the peak representing ^{123}I-mIBG (retention time of ~11 min).

The PBMC curve (fitted using the parent fraction data of all subjects) and all IMC curves are shown in Figure 4. The final population-based input function correction curve with both BPR correction and PBMC was obtained by dividing the PBMC curve with the BPR curve. The detailed values for the BPR correction, PBMC, and the final population-based input function correction curves are shown in Table 1. The fitting equations of BPR and PBMC are reported in the supplemental data (supplemental materials are available at http://jnm.snmjournals.org).


FIGURE 3. Sample metabolite chromatograms from healthy human. x-axis is high-performance liquid chromatography retention time, and y-axis is counting rate of γ-signals.

Kinetic Modeling Results

The dynamic ^{123}I-mIBG SPECT studies for the healthy humans indicated that the washout of ^{123}I-mIBG in the myocardium was minimal in this healthy population. A representative myocardial time–activity curve and input function from 1 subject are shown in Figure 5. The 2T compartment model provided a

FIGURE 2. Population-based BPR curve.
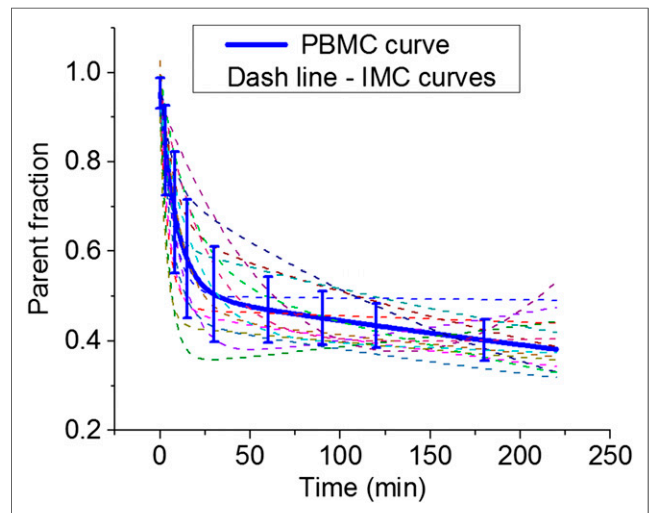
FIGURE 4. PBMC and IMC curves of 12 healthy human subjects. Error bars of PBMC curve are ±SD values calculated with Equation 2. PBMC values are 95.3% ± 3.4%, 82.6% ± 10.1%, 68.7% ± 13.6%, 58.4% ± 13.2%, 50.5% ± 10.6%, 47.0% ± 7.4%, 45.2% ± 5.9%, 43.5% ± 5.0%, and 40.2% ± 4.6% at 0, 3, 8, 15, 30, 60, 90, 120, and 180 min after injection.

TABLE 1
Population-Based Correction Curve Values for Image-Derived Input Function

Correction	Time (min)								
	0	3	8	15	30	60	90	120	180
BPR	0.23	1.37	1.99	2.06	1.80	1.47	1.35	1.30	1.27
PBMC	0.95	0.83	0.69	0.58	0.50	0.47	0.45	0.43	0.40
Both corrections	4.13	0.61	0.35	0.28	0.28	0.32	0.33	0.33	0.32

slightly better fit of the myocardial time–activity curve than 1T and 2Ti models with both BPR correction and PBMC (Akaike information criterion values for this subject were −0.6, −2.8, and 1.4 for 1T, 2T, and 2Ti models, respectively). However, differences in Akaike information criterion between 2T and the other 2 models with both BPR correction and PBMC were insignificant for all 12 subjects ($P = 0.96$ for 2T vs. 1T and $P = 0.90$ for 2T vs. 2Ti using paired t test). In our previous analysis of ^{123}I-mIBG studies in 4 HF patients and a dog with more substantial myocardial washout, the 2T appeared to provide a significantly better fit to the data than the 1T model. The dog study also suggested an improved fit over the 2Ti model (reported in the supplemental data) (21). Therefore, in the current study we chose the 2T as the optimized model for the following kinetic modeling for consistency.
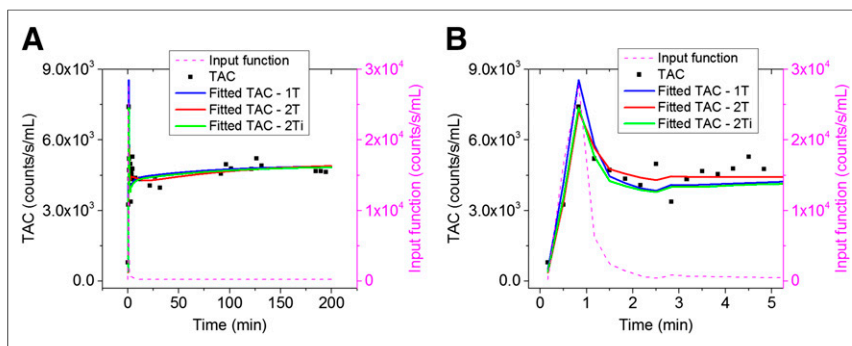
Sample fitting results of the myocardial time–activity curve using the 2T model without any corrections, with both BPR correction and PBMC and with both BPR correction and IMC for the input functions, are shown in Figure 6. The 2T model without any corrections for the input function does not fit the myocardial time–activity curve well. The application of BPR correction and PBMC on the input function improved the fitting visually, which was similar to the fitting result with BPR correction and IMC. V_T values derived without and with corrections for the input functions using the 2T model for all 12 healthy individual subject studies are summarized in Table 2 and the average normal values displayed graphically with results of the paired t test comparisons between groups in Figure 7. When both BPR correction and PBMC were applied to the image-derived input function, the mean V_T value (±SD) was $29.0 ± 12.4$ mL/cm^3, and the mean blood volume value (±SD) to correct for spill-in from the left ventricle blood pool was $0.30 ± 0.11$ mL/cm^3. The V_T values ranged from 15.0 to 53.8 mL/cm^3 with both BPR correction and PBMC, which was increased by $188% ± 32%$ compared with those obtained without

any corrections on the input functions. There was a significant difference between V_T values obtained with only PBMC and with both BPR correction and PBMC ($P = 2.3e-04$), indicating that the BPR correction is needed for quantitative analysis of dynamic ^{123}I-mIBG SPECT images. There was also a significant difference between V_T values obtained with only BPR correction compared with both BPR correction and PBMC ($P = 1.6e-05$), indicating that metabolite correction is necessary for ^{123}I-mIBG kinetic modeling. With BPR correction on the input function, the V_T difference between PBMC and IMC ranged from −14% to 13% (−3% ± 8%). The difference between the V_T values obtained with these 2 methods was insignificant ($P = 0.39$). In addition, the intersubject coefficient of variation values after PBMC (43%) and IMC (42%) were similar, indicating that PBMC is a reasonable surrogate for a subject-specific metabolite correction in the analysis of dynamic ^{123}I-mIBG images. The large coefficient of variation values might be caused by the large intersubject variation of ^{123}I-mIBG uptake in the healthy population and the high noise level in the dynamic ^{123}I-mIBG SPECT images.

DISCUSSION

Our study demonstrated the feasibility of 4D dynamic ^{123}I-mIBG SPECT imaging with tracer kinetic modeling using a stationary dedicated cardiac CZT SPECT/CT scanner. To our knowledge, this is the first report of normal myocardial V_T values using quantitative ^{123}I-mIBG SPECT imaging in a group of healthy human subjects. Fewer scans over a shorter time interval could be feasible for clinical application of this technique (reported in the supplemental data), although further investigations are needed for the optimization of simplified imaging protocol. The linear correlation ($R^2 = 0.89$) between the V_T values with and without attenuation correction (reported in the supplemental data) might be applied to the cardiac SPECT systems without a registered CT, potentially leading to a broader impact of this technique in clinical application, due to the large installation base of SPECT-only scanners.

Both a BPR correction and a metabolite correction of the image-derived input function are needed for accurate kinetic modeling of dynamic ^{123}I-mIBG images. The ex vivo tissue metabolite analysis in a dog (reported in the supplemental data) showed that at 180 min after tracer injection radiolabeled metabolites of ^{123}I-mIBG were found in the kidney and liver, although no radiolabeled metabolites were detected in the left ventricle and left atrium. These data suggest that the SPECT images should

FIGURE 5. Sample time–activity curve (TAC) fitting results of normal human using different compartment models for total 3 h (A) and first 5 min (B).
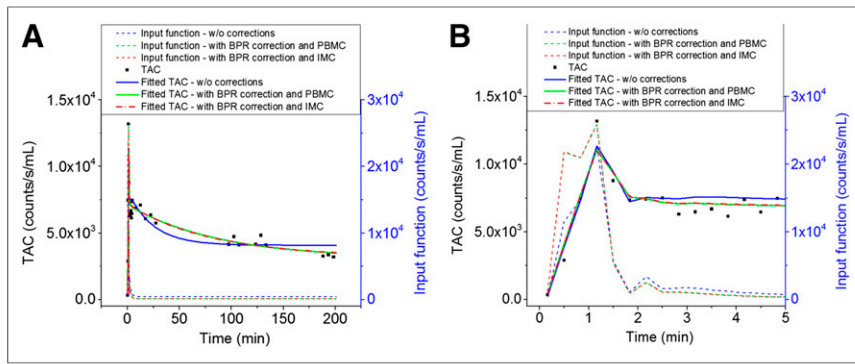
FIGURE 6. Sample time–activity curve (TAC) fitting results of myocardium for human subject without and with corrections for input functions for total 3 h (A) and first 5 min (B). Fitted time–activity curve with BPR correction and PBMC overlapped with fitted time–activity curve with BPR correction and IMC.

reflect the true distribution of ^{123}I-mIBG in the myocardium. In the current study, serial venous blood samples were taken for metabolite analysis. Although arterial blood sampling is usually desirable for metabolite analysis in tracer kinetic modeling studies, the expense and risk of this procedure limits the routine clinical measurement of a true arterial input function from serial arterial samples. In our pilot preclinical dog studies reported in the supplemental data, we showed that the V_T difference between arterial IMC and venous PBMC was in the range of -8% to 16%. We might anticipate an even smaller variation for humans because our studies demonstrate that the magnitude of ^{123}I-mIBG metabolism was greater in dogs. This suggests that the venous PBMC method proposed in this study should be reasonably accurate for humans, although further investigations are needed. No significant difference in V_T values was observed between our PBMC and our

subject-specific IMC, indicating that the PBMC is feasible for ^{123}I-mIBG kinetic modeling studies. We reported both BPR and PBMC data that can be used in future clinical studies with dynamic ^{123}I-mIBG SPECT imaging, without the need to draw blood samples and to perform high-performance liquid chromatography analysis for each individual patient. The correlation study of V_T values (using 2T model) between without any corrections on the input function and with both BPR correction and PBMC was further performed in the supplemental data, indicating a strong linear correlation ($R^2 = 0.94$) between these 2 groups. The correlation function determined in this study could be used in future clinical studies to scale the V_T values without those corrections, as an alternative to population-based input function corrections. However, it might be necessary to first demonstrate that the HF patients metabolize ^{123}I-mIBG similar to our normal controls. The recent human dynamic PET imaging studies with ^{11}C-metahydroxyephedrine (^{11}C-HED) (22), a norepinephrine analog for PET imaging with an uptake mechanism similar to ^{123}I-mIBG, have shown a relatively larger error (up to 30%) in tracer kinetic modeling results when population-averaged metabolite correction was applied than with individual metabolite correction. The reason for this increased error could be the relatively lower parent fraction of ^{11}C-HED ($<20\%$ at 60 min after injection) than ^{123}I-mIBG ($>40\%$ at 60 min after injection). This difference in metabolism could explain the relatively larger variation that was seen in the metabolism of ^{11}C-HED among different individuals than ^{123}I-mIBG.

TABLE 2
V_T Values for 12 Healthy Human Subjects

Subject	V_T^1	V_T^2	V_T^3	V_T^4	V_T^5	$\frac{V_T^4-V_T^1}{V_T^1}$	$\frac{V_T^4-V_T^5}{V_T^5}$
1	9.0	11.9	18.8	23.7	23.6	162%	0%
2	9.1	12.5	17.3	22.2	21.1	144%	5%
3	5.2	6.2	11.1	15.0	17.0	190%	−12%
4	8.4	11.7	18.2	25.3	29.4	202%	−14%
5	6.1	9.1	18.0	19.1	19.6	212%	−2%
6	11.7	15.7	27.6	37.3	37.0	218%	1%
7	15.8	21.3	39.3	53.8	47.7	240%	13%
8	16.2	23.9	32.9	49.3	56.5	204%	−13%
9	10.3	10.5	23.6	26.3	26.0	154%	1%
10	11.7	14.2	28.2	36.2	39.0	210%	−7%
11	6.6	9.2	13.8	18.7	18.2	183%	3%
12	8.9	9.9	15.1	21.6	23.3	141%	−7%
Mean	9.9	13.0	22.0	29.0	29.9	188%	−3%
SD	3.5	5.2	8.5	12.4	12.6	32%	8%

$V_T^1 = V_T$ without any correction on the input function; $V_T^2 = V_T$ with BPR correction only; $V_T^3 = V_T$ with PBMC only; $V_T^4 = V_T$ with both BPR correction and PBMC; $V_T^5 = V_T$ with both BPR correction and IMC.
Values are given in mL/cm^3.
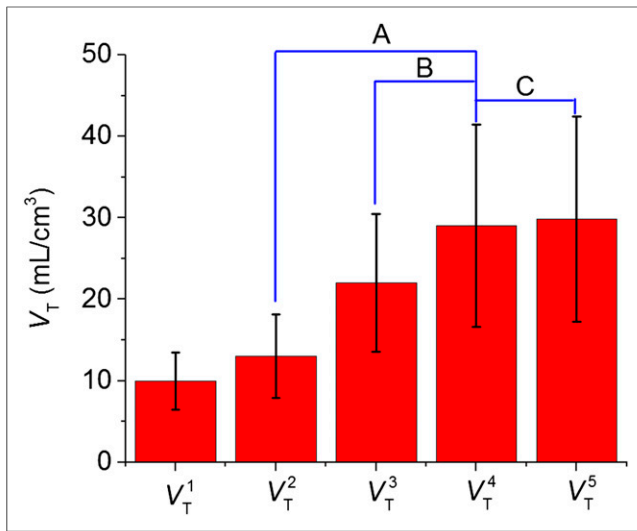
FIGURE 7. Mean and SD for V_T values in Table 2. Paired t test results are $P = 1.6e-05$ (A), $P = 2.3e-04$ (B), and $P = 0.39$ (C). P value smaller than 0.05 indicates statistical significance.

The 2T compartment model was selected as the optimal model for kinetics analysis of ^{123}I-mIBG, because this approach appears to provide curve fitting results superior to the 1T and 2Ti models based on our previous analysis of ^{123}I-mIBG studies in HF patients and dogs with more substantial myocardial washout (*21*). However, differences in Akaike information criterion between 2T and the other 2 models were insignificant for all 12 healthy subjects in our studies. It is possible that simpler models such as the 1T model could provide V_T values with smaller variability for this normal population. Myocardial V_T values in healthy human subjects ranged from 15.0 to 53.8 mL/cm^3 (29.0 ± 12.4 mL/cm^3). Our establishment of a normal database for the volume of retention of ^{123}I-mIBG in the myocardium may be valuable in future patient studies, in which V_T values below 15 mL/cm^3 might be used to predict cardiac events. Additional dynamic ^{123}I-mIBG SPECT imaging studies in HF patients are needed to identify the typical V_T values in this important patient population.

The initial results derived from our dynamic ^{123}I-mIBG imaging studies in dogs reported in the supplemental data showed that the specific volume of distribution accounted for 90% of V_T in the dog myocardium, which is consistent with the prior studies demonstrating that there is little nonspecific uptake of ^{123}I-mIBG in human heart (*23*). The dynamic PET studies also reported that V_T approximated the specific volume of distribution of ^{11}C-HED in the human heart (*22*). On the basis of these results, V_T should be considered as the appropriate parameter for measurement of cardiac sympathetic activity.

It is believed that the HMR is a surrogate measurement of V_T. Therefore, we expect V_T values obtained from dynamic SPECT imaging will be more accurate than HMR from 2D planar imaging to quantify sympathetic activity. For the healthy population in this study, the typical WOR values were close to zero. In future studies of patients with HF typically demonstrating a decreased myocardial uptake and a greater myocardial WOR, we will need to establish the correlation between V_T and HMR (or WOR) to demonstrate the true clinical value of the proposed dynamic 4D imaging method compared with the conventional 2D planar imaging approach.

Further investigations are needed to evaluate the test–retest reproducibility of this 4D dynamic ^{123}I-mIBG SPECT imaging method. The possible issues for the reproducibility will be the high noise level of dynamic SPECT images and the consistency in the positioning of the myocardial and blood-pool VOIs for multiple scans. In addition, the physiology in the target HF population (less uptake and more rapid clearance) is different from normal controls and this may affect reproducibility and might need changes in the imaging protocol. The HF patients with abnormal renal or liver function might have metabolite characteristics different from those in normal subjects, which need to be further investigated in the future.

CONCLUSION

Absolute quantification of dynamic ^{123}I-mIBG SPECT imaging is feasible using a stationary dedicated cardiac CZT SPECT/CT scanner with application of statistical iterative reconstruction and data corrections. The V_T values (range, 15.0–53.8 mL/cm^3; mean, 29.0 ± 12.4 mL/cm^3) of ^{123}I-mIBG were first reported for healthy humans. Substantial radiolabeled metabolites of ^{123}I-mIBG were detected in the plasma of humans, and both a BPR correction and a metabolite correction are needed for absolute quantification of dynamic ^{123}I-mIBG SPECT imaging. We have developed a population-based BPR correction method and a population-based metabolite correction method, which could be used in the analysis of future clinical dynamic ^{123}I-mIBG SPECT images without the need for the analysis of blood samples in individual subjects.

REFERENCES

1. Verberne HJ, Brewster LM, Somsen GA, van Eck-Smit BLF. Prognostic value of myocardial ^{123}I-metaiodobenzylguanidine (MIBG) parameters in patients with heart failure: a systematic review. *Eur Heart J.* 2008;29:1147–1159.
2. Travin MI. Cardiac neuronal imaging at the edge of clinical application. *Cardiol Clin.* 2009;27:311–327.
3. Raffel DM, Wieland DM. Development of mIBG as a cardiac innervation imaging agent. *JACC Cardiovasc Imaging.* 2010;3:111–116.
4. Jacobson AF, Senior R, Cerqueira MD, et al. Myocardial iodine-123 meta-iodobenzylguanidine imaging and cardiac events in heart failure results of the prospective ADMIRE-HF (AdreView Myocardial Imaging for Risk Evaluation in Heart Failure) study. *J Am Coll Cardiol.* 2010;55:2212–2221.
5. Okuda K, Nakajima K, Hosoya T, et al. Semi-automated algorithm for calculating heart-to-mediastinum ratio in cardiac iodine-123 MIBG imaging. *J Nucl Cardiol.* 2011;18:82–89.

6. Nakajima K, Nakata T. Cardiac ^{123}I-mIBG imaging for clinical decision making: 22-year experience in Japan. *J Nucl Med.* 2015;56(suppl 4):11S–19S.

7. van der Veen BJ, Younis I, de Roos A, Stokkel MM. Assessment of global cardiac I-123 MIBG uptake and washout using volumetric quantification of SPECT acquisitions. *J Nucl Cardiol.* 2012;19:752–762.

8. Chen J, Folks R, Verdes L, Manatunga D, Jacobson A, Garcia E. Quantitative I-123 mIBG SPECT in differentiating abnormal and normal mIBG myocardial uptake. *J Nucl Cardiol.* 2012;19:92–99.

9. Travin MI. Cardiac radionuclide imaging to assess patients with heart failure. *Semin Nucl Med.* 2014;44:294–313.

10. Kasama S, Toyama T, Iwasaki T, et al. Evaluation of cardiac sympathetic nerve activity and aldosterone suppression in patients with acute decompensated heart failure on treatment containing intravenous atrial natriuretic peptide. *Eur J Nucl Med Mol Imaging.* 2014;41:1683–1691.

11. Dimitriu-Leen AC, Scholte AJHA, Jacobson AF. ^{123}I-mIBG SPECT for evaluation of patients with heart failure. *J Nucl Med.* 2015;56(suppl 4):25S–30S.

12. Arimoto T, Takeishi Y, Fukui A, et al. Dynamic ^{123}I-mIBG SPECT reflects sympathetic nervous integrity and predicts clinical outcome in patients with chronic heart failure. *Ann Nucl Med.* 2004;18:145–150.

13. Tinti E, Positano V, Giorgetti A, Marzullo P. Feasibility of ^{123}I-meta-iodobenzylguanidine dynamic 3-D kinetic analysis in vivo using a CZT ultrafast camera: preliminary results. *Eur J Nucl Med Mol Imaging.* 2014;41:167–173.

14. Giorgetti A, Burchielli S, Positano V, et al. Dynamic 3D analysis of myocardial sympathetic innervation: an experimental study using ^{123}I-mIBG and a CZT camera. *J Nucl Med.* 2015;56:464–469.

15. Innis RB, Cunningham VJ, Delforge J, et al. Consensus nomenclature for in vivo imaging of reversibly binding radioligands. *J Cereb Blood Flow Metab.* 2007;27:1533–1539.

16. Fan P, Hutton BF, Holstensson M, et al. Scatter and crosstalk corrections for ^{99m}Tc/^{123}I dual-radionuclide imaging using a CZT SPECT system with pinhole collimators. *Med Phys.* 2015;42:6895–6911.

17. Chan C, Dey J, Grobshtein Y, et al. The impact of system matrix dimension on small FOV SPECT reconstruction with truncated projections. *Med Phys.* 2016;43:213–224.

18. Lin SF, Labaree D, Chen MK, et al. Further evaluation of [^{11}C] MP-10 as a radiotracer for phosphodiesterase 10A: PET imaging study in rhesus monkeys and brain tissue metabolite analysis. *Synapse.* 2015;69:86–95.

19. Gunn RN, Gunn SR, Cunningham VJ. Positron emission tomography compartmental models. *J Cereb Blood Flow Metab.* 2001;21:635–652.

20. Marquardt DW. An algorithm for least-squares estimation of nonlinear parameters. *J Soc Indust Appl Math.* 1963;11:431–441.

21. Prasad R, Thorn S, Chan C, et al. Quantification and kinetic modeling of ^{123}I-mIBG using dynamic SPECT for cardiac innervation [abstract]. *J Nucl Med.* 2015;56(suppl 3):408.

22. Harms HJ, de Haan S, Knaapen P, et al. Quantification of [^{11}C]-meta-hydroxyephedrine uptake in human myocardium. *EJNMMI Res.* 2014;4:52.

23. David MR. Targeting norepinephrine transporters in cardiac sympathetic nerve terminals. In: Welch MJ, Eckelman WC, eds. *Targeted Molecular Imaging.* Boca Raton, FL: Taylor & Francis; 2012:305–320.